ELSEVIER

Journal of Alloys and Compounds 408–412 (2006) 1065–1070

Journal of ALLOYS AND COMPOUNDS

www.elsevier.com/locate/jallcom

Neutron studies of rare earth-modified zirconia catalysts and yttrium-doped barium cerate proton-conducting ceramic membranes

Chun-Keung Loong [a,*], Masakuni Ozawa [b], Ken Takeuchi [c], Koichi Ui [c], Nobuyuki Koura [c]

[a] *Argonne National Laboratory, IPNS-360, Argonne, IL 60439, USA*
[b] *Nagoya Institute of Technology, Tajimi, Gifu, Japan*
[c] *Tokyo University of Science, Oshamanbe, Hokkaido and Noda, Chiba, Japan*

Received 30 July 2004; received in revised form 15 November 2004; accepted 15 December 2004
Available online 1 August 2005

Abstract

The techniques of neutron scattering were applied to characterize two rare-earth containing ceramic systems: oxide-based automotive three-way catalysts and proton-conducting cerate-perovskite-based hydrogen-separation membranes. High-surface-area zirconias are widely used as catalytic support of noble metals in automotive three-way catalytic converters for exhaust gas treatment. Doping these oxides with rare-earth elements provides an important means in tailoring their properties for better catalytic performance. We have carried out in situ small-to-wide angle neutron diffraction at high temperatures and under controlled atmospheres to study the sintering behavior and the $Ce^{3+} \leftrightarrow Ce^{4+}$ redox process in $Ce_xZr_{1-x}O_{2-\delta}$ solid solutions dispersed with Pt nanoparticles. We found substantial effects due to RE-doping on the nature of aggregation of nanoparticles, defect formation, crystal phase transformation, and metal-support interaction. Y-doped $BaCeO_3$ exhibits significant proton conductivity under a hydrogen-containing atmosphere at high temperatures. This system has high potential for applications as fuel-cell electrolytes, gas sensors, and ceramic membranes for hydrogen separation. We have performed in situ neutron diffraction to obtain information regarding the crystal phase evolution that permits dissolution of hydrogen and proton migration through the lattice. Neutron quasielastic- and inelastic-scattering experiments were carried out to investigate the proton dynamics from local vibrations to long-range diffusion.

Keywords: Three-way catalyst; Neutron scattering; Proton-conducting pervoskite; Rare-earth modified zirconia; Yttrium-doped barium cerate

1. Introduction

Complex oxides containing rare-earth (RE) elements exhibit rich varieties of physical and chemical properties that deserve systematic experimental characterization over multiple length and time scales. Information regarding the time-averaged structure, from atomic/molecular locations to microstructure and morphology of crystalline or amorphous domains, provides a first notion on the organization of the microscopic build blocks in the materials. Of equal importance are the collective, diffusive, and vibrational motions of atoms and molecules that are responsible to various thermodynamic behavior. Photons, electrons and neutrons are the common scattering and/or imaging probes whereby space–time density–density correlation functions are obtained in real (space $\vec{r}$ and time t) and/or reciprocal (scattering vector $\vec{Q}$ and energy E) space. Slow neutrons differ from electrons and photons (visit light to X-rays) in their much lower energies ($\ll$1 eV) while matching the wavelengths with the interatomic spacing and molecular dimensions of condensed matter. Neutrons interact with atomic nuclei (nuclear scattering) and electronic or nuclear spins (magnetic scattering) in the bulk of the materials and, for RE materials, the latter plays a key role in studying the magnetism of 4f electrons. In this paper, we present recent neutron-scattering studies of the structures and dynamics of atoms in two classes of RE complex oxides: high-surface-area auto-

* Corresponding author. Tel.: +1 630 252 5596; fax: +1 630 252 4163.
E-mail address: ckloong@anl.gov (C.-K. Loong).

0925-8388/$ – see front matter © 2005 Published by Elsevier B.V.
doi:10.1016/j.jallcom.2004.12.195

motive three-way catalysts (TWC) and proton-conducting pervoskites. They share an important common characteristic, namely, the presence of defects in a crystalline structure induced by partial substitution of a cationic species with a RE element. The consequences in the functionality of the materials are critical. It will be shown that neutron-scattering investigations yielded helpful clues to the structure-function relation of these materials.

2. Neutron scattering experiments

The nuclear-scattering cross-section of slow neutrons from an element containing natural isotopic abundance and uncorrelated distribution of nuclear spins can be quantitatively described by a coherent scattering length b, which in most cases is a real number. The fact that b does not depend in any regular fashion on the atomic or nuclear charges, e.g., $b_H = -0.374$, $b_O = 0.58$, $b_{ce} = 0.484$ for hydrogen, oxygen, and cerium, respectively, in units of 10^{-12} cm, is a distinct advantage for the discern of light versus heavy atoms or adjacent elements in the periodic tables within a compound or alloy. Furthermore, accurate determination of the crystal structures of different phases and the defects associated with oxygen-ion vacancies are benefited by the relatively large scattering length for oxygen.

At small Q ($\sim 10^{-3}$ to 10^{0} Å^{-1}), small-angle neutron scattering (SANS) is sensitive to relatively large ($\sim$1–100 nm) particles with relatively low resolution ($\sim$1 nm). For a monodisperse system, it can be shown [1] that the elastic-scattering cross-section is a product of the particle form factor $P(Q)$ and interparticle structure factor $S(Q)$:

$$\frac{d\sigma(Q)}{d\Omega} \propto \bar{\rho} P(Q) S(Q) \quad (1)$$

where $\bar{\rho}$ is the contrast factor which amounts to the square of the difference in the mean scattering–length density between the particles and the background (e.g., voids) and Ω is the solid angle of the detector. The aim of a SANS experiment is to determine the size and shape of the particles from $P(Q)$ and their spatial distribution from $S(Q)$. Neutron diffraction at increasing Q probes the spatial arrangement of structural units at progressively decreasing length scales. Eventually, high-resolution scattering data covering a Q range of $\sim$1–50 Å^{-1} allow the determination of the time-averaged (static) atomic organization: the atom type, position, and occupation number. For mono- or polycrystalline materials, a reconstruction of a three-dimensional atomic lattice can be achieved by well-known crystallographic methods. Intensity appearing between the Bragg peaks, termed diffuse scattering, can be analyzed to infer the nature of the defect structure. Fig. 1 displays schematically the features expected for a nanostructured crystalline powder.

A neutron spectrometer is capable of analyzing the neutron energy transfers E over a range of Q. As a result, inelastic neutron scattering (INS) data are described in general by a scattering function $S(\vec{Q}, E)$. It can be shown that $S(\vec{Q}, E)$ is connected to the space–time particle–particle correlation functions through a double Fourier transform[1]. The time and length scales probed by neutron spectroscopy are typically on the range of 10^{-8} to 10^{-13} s and 0.01–10 Å, respectively. The random distribution of isotopes and their nuclear spin directions of an element give rise to another kind of scattering termed incoherent scattering of which the scattered wavefronts from different atoms do not interfere, thereby yielding no structural information. However, for inelastic scattering the incoherent intensities represent the uncorrelated single-particle dynamic response of the elements over the $(\vec{Q}, E)$ domain. Owing to spin incoherence, hydrogen has an extraordinary large incoherent scattering cross-section ($\sigma_{inc} = 4\pi b_{inc}^2$) of $\sim 80 \times 10^{-24}$ cm^2 when compared to other elements (e.g., 0.49 and 0.03 in units of 10^{-24} cm^2 for N and Ca, respectively, and zero for C and O). Therefore, INS and quasielastic neutron scattering (QENS) are well suited to study local vibrations and diffusion of hydrogen in materials.

3. Rare-earth modified oxides for automotive catalytic supports

High-surface-area zirconias are widely used as catalytic support of noble metals in automotive exhaust-emission-control systems. Doping zirconia with a small amount of RE may tailor its properties for better catalytic performance [2,3]. We studied a series of $RE_xZr_{1-x}O_{2-\delta}$ (RE = La, Ce and Nd, $0 \le x \le 0.2$; BET surface area: 26–130 m^2/g) with and without the dispersion of Pt nanoparticles that were prepared by a coprecipitation technique at relatively low calcination temperature (up to 600 °C) so that the nanostructural architecture of the powders are preserved [4], as shown by a typical electron microscopy in Fig. 1a. First, SANS measurements identified the microstructure of such powders in terms of aggregation of primary particles in a fractal-like morphology of which the particle size distribution, interfacial roughness, and fractal dimension over the length scale of $\sim$1–100 nm were determined according to the RE element and concentration as well as the history of heat treatment (see Fig. 1b) [5]. In general, RE-doping increases the thermal stability against sintering and preserves the high-surface-area morphology of the powder up to about 800 °C—the typical upper operation temperature of a three-way catalytic converter in an automobile. Secondly, it is well known that RE-doping stabilizes the crystal structures at ambient temperature to avoid the disruptive formation of the monoclinic phase as in pure zirconia. Neutron powder diffraction, see for example Fig. 1c, established the molar fraction of the metastable cubic and tetragonal phases and the crystallite domain size in $RE_xZr_{1-x}O_{2-\delta}$ as a function of heat-treatment temperature [6]. Thirdly, substituting Zr^{4+} ions with trivalent RE such as Nd^{3+} and Y^{3+} results in defect

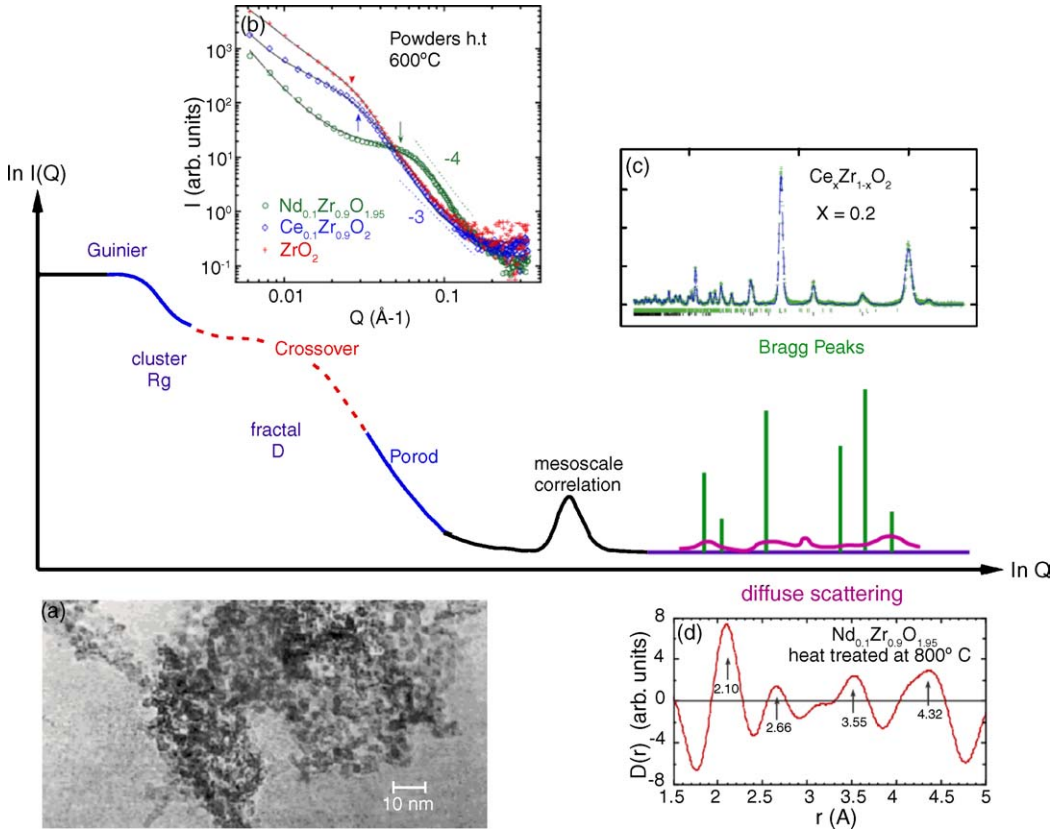

Fig. 1. Small-to-high angle diffraction shown schematically for the measurement of density-density correlation weighted by the neutron scattering-length density of the constituent atoms. As Q increases, the correlation length decreases from sub-micron size clusters (Guinier region) to a crossover to aggregation of primary particles, then to the meso-length scale and finally to interatomic distances. Structural deviations from the average crystal structure manifest in residual intensity (diffuse scattering) between the Bragg peaks. (a) A TEM micrograph showing a typical nanostructure of RE-modified zirconia; (b) the SANS profiles of pure CeO_2 and Ce- and Nd-doped ZrO_2 characterized by a fractal-like interparticle structure factor; (c) neutron powder diffraction of $Ce_{0.2}Zr_{0.8}O_2$; (d) correlation function $D(r)$ calculated from the diffuse-scattering component. The maxima corresponds to atomic spacing characteristic of a short-range defect structure.

formation in the crystal structure associated with oxygen-ion vacancies ($\delta \cong x/2$). The diffuse residual intensities were analyzed by a Fourier filtering technique whereby a correlation function, $D(r)$, was obtained in real space. In Fig. 2d for $Nd_{0.1}Zr_{0.9}O_{1.95}$, the $D(r)$ displays four maxima at atomic spacings characteristic of short-range structure that gives rise to the diffuse scattering. The first maximum at about 2.10 ± 0.03 Å corresponds to a relaxation of the Zr(RE)-O distances along the pseudocubic ⟨1 1 1⟩ direction of the fluorite structure. There is also evidence of additional atomic

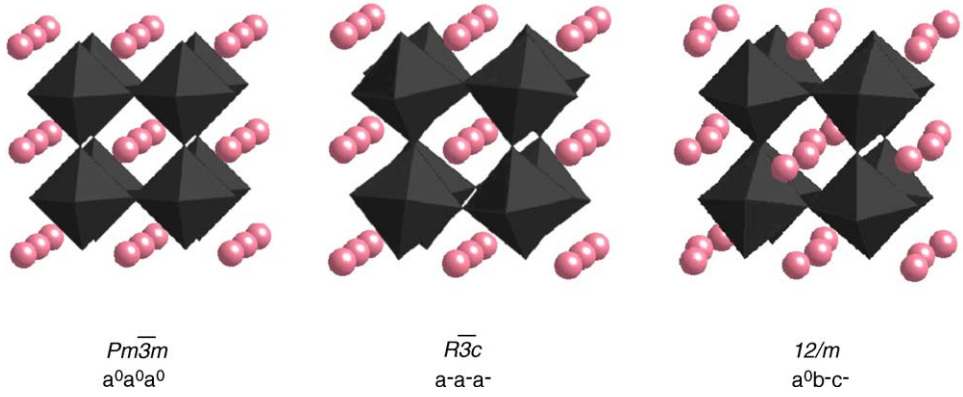

Fig. 2. The perovskite structure of BCY where the Ba atoms and CeO_6 octahedra are shown. $Pm\bar{3}m$ is the parent cubic structure. Other phases, such as the rhombohedral ($R\bar{3}c$) and the monoclinic ($I2/m$) phases, are formed by systematic tilts of the octahedra along the high-symmetry direction of the cubic structure, designated by the Glazer notion [18].

correlation at 2.66 ± 0.04, 3.55 ± 0.04, and 4.35 ± 0.05 Å [6].

The crystal and defect structures of RE-modified zirconias have been investigated by numerous workers including using single-crystal specimens. It was realized that the solid solutions are too complex to be characterized by mixing variants of the fluorite and pyrochlore phases [7]. Furthermore, an optimal utilization of the redox property of CeO_2 has very important consequences in tailoring the oxygen storage capacity for better TWC performance [8]. Harrison et al. [9] proposed a model for metal-support interaction which involves the initial adsorption of CO molecules on Pt atoms and subsequently a reduction of Ce cations in the ceria/Pt interface. The $Ce^{4+} \rightarrow Ce^{3+}$ conversion releases oxygen atoms from ceria for the oxidation of CO to CO_2, which subsequently desorbs from the metal, leaving vacancies on the surface of the oxide particles. In order to sustain the redox reaction, the vacant sites have to be filled by oxygen from the lattice through atomic diffusion. We performed in situ neutron diffraction on $Ce_{0.2}Zr_{0.8}O_{2-\delta}$ and pure CeO_2 samples with and without dispersed Pt at high temperature under oxidizing (2% O_2/Ar) and reducing (1% CO/Ar) atmosphere [10]. The conversion of Ce^{4+} to Ce^{3+} ions was monitored by the rate of increase in the lattice constants by virtue of the substantial difference in the ionic radius of Ce^{4+} (0.097 nm) and Ce^{3+} (0.114 nm). We found, under a reducing atmosphere, the conversion was more rapid in the Pt-containing $Ce_{0.2}Zr_{0.8}O_{2-\delta}$ sample. Since the observed d-spacing reflects the long-range order structure in the crystalline grains, the enhanced expansion in Pt-containing samples implies the migration of oxygen vacancies from the interfacial region between the oxide and Pt particles to the bulk of the oxide lattice. In CeO_2–ZrO_2 solid solutions without metal loading, the reduction of Ce at high temperature occurs mainly on the surface region of the sample [11,12]. However, recently Mamontov et al. [13–15] analyzed the neutron diffusion scattering from pure CeO_2 and CeO_2-rich CeO_2–ZrO_2 samples using a pair-distribution-function technique with the aid of a structural model. It was argued that reduced Ce^{3+} ions and correspondingly oxygen-ion vacancies occurred in these samples driven by the relief of internal stress due to the different ionic size of Ce^{4+} and Zr^{4+} in the solution. The authors suggested that the motion of the oxygen-ion defects is responsible to the oxygen storage capacity.

4. Yttrium-doped barium cerate proton conductors

$BaCe_{1-x}Y_xO_{3-y}$ ($0 \le x \le 0.3$) (BCY) was first synthesized by Iwahara who also reported a high total conductivity of $\approx 5.3 \times 10^{-2}\ (\Omega\,\mathrm{cm})^{-1}$ for $x = 0.2$ at 800 °C in a hydrogen-containing atmosphere [16]. Guan et al. [17] provided evidence of significantly higher H^+ conductivity than that of the O^{2-} counterpart. This makes the materials attractive for many applications, from fuel cells to hydrocarbon sensors to hydrogen pumps. At Argonne interests have been focused on the research and development of a BCY-based hydrogen-separation membrane capable of operating in a nongalvanic mode, i.e., without electrodes or power supply.

BCY belongs to the family of perovskite structures but, due to fact that sample stoichiometry and oxygen-vacancy-related defects are very sensitive to preparation and processing conditions, the crystal structure was not well understood. We demonstrated that single-phase $BaCe_{1-x}Y_xO_{3-y}$ ($0 \le x \le 0.3$) can be synthesized provided that in the final preparation step the samples are annealed in a hydrogen-free environment. Under hydrogen- or moisture-containing atmospheres including ambient air, subtle tilts of the CeO_6 octahedra result in the formation of variant structures, as shown in Fig. 2 for three major phases [18]. Taking the advantage of the high sensitivity of neutrons to oxygen atoms, we determined the crystal structures of BCY and their structural evolution subjected to exposure of different atmospheres [19]. Table 1 shows the room-temperature crystal structures of BCY that were heated treated under various conditions. We find that the O_2-annealed BCY samples crystallize into well-defined single-phase perovskite structures: orthorhombic (*Pmcn*) for $0 \le x \le 0.1$ and rhombohedral ($R\bar{3}c$) for $0.15 \le x \le 0.3$. For low *Y* concentration, $x \le 0.1$, the orthorhombic (*Pmcn*) structure is not affected by annealing in ambient air or dry 4% H_2. In this composition range, the low concentration of oxygen vacancies may limit the solubility of hydrogen, as suggested by the following proton incorporation reaction: $H_2O(g) + V_O^{\bullet\bullet} + O_O^x \rightarrow 2OH_O^{\bullet\bullet}$, where $OH_O^{\bullet}$, $V_O^{\bullet\bullet}$, and O_O^x represent the protons, oxygen vacancies, and lattice oxygen, respectively. For higher *Y* concentrations, $x > 0.1$, the rhombohedral ($R\bar{3}c$) structure is unstable in ambient air or dry 4% H_2, as evident in the appearance of a mixture of phases (see Table 1). The $x = 0.15$ composition contained monoclinic ($I2/m$) and orthorhombic (*Incn*) phases, while samples with

Table 1
The room-temperature crystal structures of $BaCe_{1-x}Y_xO_{3-\delta}$ ($0 \le x \le 3$) that were heat treated under different conditions (see text)

$BaCe_{1-x}Y_xO_{3-\delta}$	Oxygen			Laboratory air	Dry CO_2-free air	Dry 4% H_2 + N_2
x	Dry	+D_2O	+H_2O			
0.00	*Pmcn*			*Pmcn*		*Pmcn*
0.10	*Pmcn*			*Pmcn*		*Pmcn*
0.15	$R\bar{3}c$			*Incn* (0.81) + $I2/m$ (0.19)		*Incn* (0.75) + $I2/m$ (0.25)
0.20	$R\bar{3}c$	Mostly $I2/m$	Mostly $I2/m$	$R\bar{3}c$ (0.14) + $I2/m$ (0.86)	$R\bar{3}c$	$R\bar{3}c$ (0.84) + $I2/m$ (0.16)
0.25	$R\bar{3}c$			$R\bar{3}c$ (0.48) + $I2/m$ (0.52)		$R\bar{3}c$ (0.53) + $I2/m$ (0.47)
0.30	$R\bar{3}c$			$R\bar{3}c$		$R\bar{3}c$ (0.71) + $I2/m$ (0.29)

The molar fractions are given in parentheses.

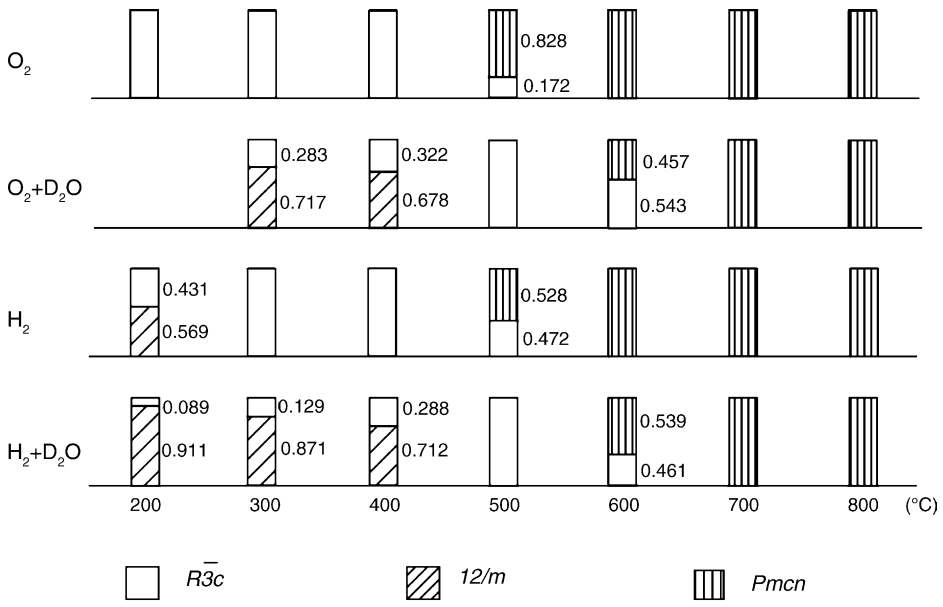

Fig. 3. Evolution of the crystal phases of $BaCe_{0.8}Y_{0.2}O_{3-y}$ at elevated temperatures under different atmospheric conditions.

$x \geq 0.2$ consisted of monoclinic ($I2/m$) and rhombohedral ($R\bar{3}c$) phases.

Based on the fact that electrical conductivity of BCY decreases for $x > 0.2$ while the concentration of $R\bar{3}c$ increases (hence a reduced $I2/m$ content, see Table 1) we suggest that the $R\bar{3}c$ phase does not favor dissolution of protons and consequently, does not lead to high electrical conductivity. The effects of hydrogen doping on the crystal structure are most evident in the $x = 0.2$ sample that was annealed in wet oxygen. Without exposure to water during annealing, a rhombohedral ($R\bar{3}c$) phase formed. If water was present during annealing, the monoclinic ($I2/m$) became the dominant structure. This fact, in conjunction with the significantly higher $I2/m$ concentration in samples that were annealed in moisture-containing laboratory air than in samples that were annealed in 4% H_2 (balance N_2), indicates that an atmosphere containing water vapor is more effective for proton doping. This is also consistent with the higher hydrogen permeation rates observed under wet conditions.

Recently, we have extended the diffraction study on $BaCe_{0.8}Y_{0.2}O_{3-y}$ to in situ measurements under pure O_2, $O_2 + D_2O$ vapor, pure H_2, and $H_2 + D_2O$ vapor at high temperatures. The overall result is presented in Fig. 3, which suggests the following scenario. Below about 500 °C the parent rhombohedral ($R\bar{3}c$) structure has too small a unit-cell volume to accommodate dissolution of hydrogen (deuterium) as hydroxyl ions in the lattice. Hydrogen dissolution is made possible by the formation of the monoclinic ($I2/m$) phase, which has a larger unit-cell volume. Furthermore, the capacity is higher for moist atmosphere than for pure hydrogen. As temperature increases from room temperature, protons are released from the hydroxyl ions as indicated by the decreasing $I2/m$ molar fraction. At ~500 °C the combination of volume expansion and the increasing thermal energy apparently suffice to initiate proton diffusion. At the same time, the lattice transforms to the cubic ($Pm\bar{3}m$) phase, which at subsequent higher temperatures, supports proton conduction.

While in situ neutron diffraction permits the characterization of the structural response of the BCY lattice to hydrogen dissolution and proton conduction, the motion of the hydrogen atoms can be monitored by concurrent spectroscopic measurements [20]. Fig. 4 shows the mean-square displacement of the hydrogen atoms as a function of temperature, obtained from integrating the incoherent elastic intensity from the dissolved hydrogen atoms in BCY recorded by detectors covering a range of Q values and fit the result to the expression of $I_{el} \propto \exp(-\langle u^2 \rangle Q^2)$. It indicates that the rate of mean-square displacement of hydrogen changes at about 360 °C, at which the depletion of the $I2/m$ phase begins. Above ~500 °C, local vibrations are replaced by diffusion as proton conduction takes over. This is evidenced by the

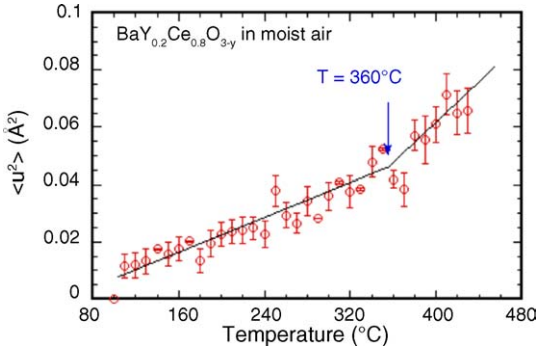

Fig. 4. The observed mean-square displacements of hydrogen atoms associated with the dissolved hydroxyl ions in $BaCe_{0.8}Y_{0.2}O_{3-y}$ in moist air as a function of temperature. A change in the rate at about 360 °C corresponds to the starting depletion of the $I2/m$ phase and activation of proton diffusion.

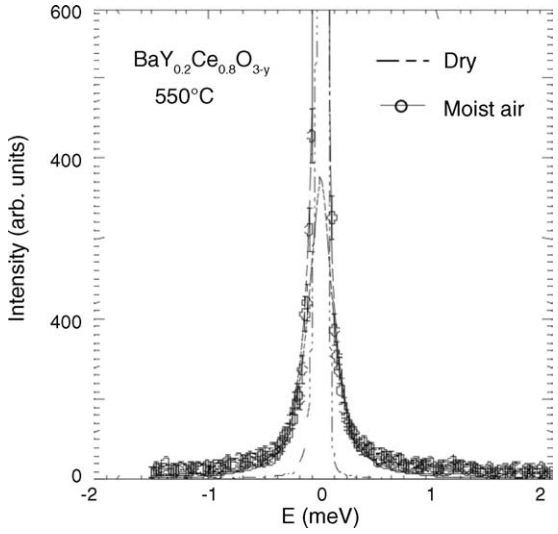

Fig. 5. The observed quasielastic scattering due to proton diffusion in $BaCe_{0.8}Y_{0.2}O_{3-y}$ at 500 °C in moist air.

appearance of a quasielastic scattering component as shown in Fig. 5. The Q-dependence of the observed quasielastic scattering can be analyzed with jump diffusion models such as that used for a similar study of Y-doped $SrCeO_3$ [21].

5. Conclusions

RE-containing complex oxides encompass a realm of material systems that exhibit outstanding chemical, optical, magnetic and transport properties. The method of neutron scattering offers a multiscale characterization of many of these fundamental properties. We describe the application of small-to-wide angle diffraction and inelastic scattering for the study of two systems: Ce-doped zirconia TWC for automotive emission control and yttrium-doped barium cerate membranes for hydrogen separation. Combining other experimental data and theoretical analyses, the knowledge acquired through these investigations is important to the realization of the full potential of the substances and the fruition of eventual technological applications.

Acknowledgements

Work performed at Argonne National Laboratory is supported by the US DOE-Basic Energy Science under the contract No. W-31-109-ENG-38. We are indebted to many collaborators, U. Balachandran, S.E. Dorris, J. Guan, T.H. Lee, J.W. Richardson Jr., S. Suzuki, P. Thiyagarajan, and J.-M. Zanotti for their contributions in the course of the studies.

References

[1] K. Sköld, D.L. Price, in: R. Celotta, J. Levine (Eds.), Methods of Experimental Physics, A–C, Academic Press, London, 1986.
[2] A. Trovarelli, Catal. Rev.-Sci. Eng. 38 (1996) 439.
[3] J. Barbier Jr., D. Duprez, Appl. Catal. B 4 (1994) 105.
[4] M. Ozawa, M. Kimura, J. Less-Common Met. 171 (1991) 195.
[5] C.-K. Loong, P. Thiyagarajan, J. Richardson, J.W.M. Ozawa, S. Suzuki, J. Catal. 171 (1997) 498.
[6] C.-K. Loong, J.W. Richardson Jr., M. Ozawa, J. Catal. 157 (1995) 636.
[7] R.L. Withers, J.G. Thompson, P.J. Barlow, J. Solid State Chem. 94 (1991) 89.
[8] M. Ozawa, M. Kimura, A. Isogai, J. Alloys Compd. 193 (1993) 73.
[9] B. Harrison, A.F. Diwell, C. Hallett, Platinum Met. Rev. 32 (1988) 73.
[10] M. Ozawa, C.-K. Loong, Catal. Today 50 (1999) 329.
[11] H.-Y. Zhu, T. Hirata, Y. Muramatsu, J. Am. Ceram. Soc. 75 (1992) 2843.
[12] J. El Fallah, S. Boujana, H. Dexpert, A. Kiennemann, J. Najerus, O. Touret, F. Villain, F. Le Normand, J. Phys. Chem. 98 (1994) 5522.
[13] E. Mamontov, T. Egami, R. Brezny, M. Koranne, S. Tyagi, J. Phys. Chem. B 104 (2000) 11110.
[14] E. Mamontov, T. Egami, J. Phys. Chem. Solids 61 (2000) 1345.
[15] E. Mamontov, R. Brezny, M. Koranne, T. Egami, J. Phys. Chem. B 107 (2003) 13007.
[16] H. Iwahara, Solid State Ionics 77 (1995) 289.
[17] J. Guan, S.E. Dorris, U. Balachandran, M. Liu, J. Electrochem. Soc. 145 (1998) 1780.
[18] A.M. Glazer, Acta Cryst. B28 (1972) 3384.
[19] K. Takeuchi, C.-K. Loong, J.W. Richardson Jr., J. Guan, S.E. Dorris, U. Balachandran, Solid State Ionics 138 (2000) 63.
[20] Concurrent diffraction, quasielastic and inelastic scattering measurements were achieved using the QENS instrument at the Intense Pulsed Neutron Source of Argonne National Laboratory.
[21] R. Hempelmann, C. Karmonik, T. Matzke, M. Cappadonia, U. Stimming, T. Springer, M.A. Adams, Solid State Ionics 77 (1995) 152.